

Photocurrent measurements in topological insulator Bi_2Se_3 nanowiresN. Meyer,¹ K. Geishendorf,² J. Walowski,¹ A. Thomas,² and M. Münzenberg¹¹*Institute of Physics, University Greifswald, 17489 Greifswald, Germany*²*IFW Dresden, Institute for Metallic Materials, Dresden, Germany*

(Dated: 21 December 2024)

Circular photogalvanic currents are a promising new approach for spin-optoelectronics. To date, such currents have only been induced in topological insulator flakes or extended films. It is not clear whether they can be generated in nanodevices. In this paper, we demonstrate the generation of circular photogalvanic currents in Bi_2Se_3 nanowires. Each nanowire shows topological surface states. Here, we generate and distinguish the different photocurrent contributions via the driving light wave. We separate the circular photogalvanic currents from those due to thermal Seebeck effects, through controlling the laser light polarization. The results reveal a spin-polarized surface-Dirac electron flow in the nanowires arising from spin-momentum locking and spin-orbit effects. The second photocurrent contribution described in this letter is caused by the thermal Seebeck effect. By scanning the photocurrent, it can be spatially resolved; upon reversing the gradient direction along the nanowire, the photocurrent changes its sign, and close to the gold contacts, the amplitudes of the different photocurrent contributions are affected by the proximity to the contacts. In the center of the nanowires, where the effects from the gold contact/ topological insulator stacks vanish, the spin-polarized current remains constant along the nanowires. This opens up a new method of all-optical spin current generation in topological insulator nanowires and hybrid structures for nanoscale spin-orbitronics.

Keywords: topological insulator, photocurrent, nanowire, circular photogalvanic effect, Seebeck effect

In the last decade, a new class of topological matter, the so-called quantum spin Hall (QSH) insulators or topological insulators (TIs), theoretically predicted in 2005 by Kane and Mele and realized in 2D in 2007 by König et al. in CdTe/HgTe quantum wells^{1,2}, has attracted great attention. This class of matter has the interesting property of an energy gap between the valence and conduction bands that is closed at the boundaries by gapless surface states with high mobility and strong spin polarization³. The surface states are predicted to be topologically protected, since their origin lies in intrinsic bulk properties such as large spin-orbit coupling, opposite parity of the bulk bands, band inversion and time-reversal symmetry, which suppresses backscattering and thereby decreases the sensitivity to surface impurities or defects. Additionally, the direction of the spin and momentum for the surface states are locked, giving rise to a strong spin polarization that makes these materials very interesting for spintronic applications e.g. as spin injectors⁴.

After the first realization of a 1D topologically non-trivial edge state, 3D topological insulators consisting of $\text{Bi}_{1-x}\text{Sb}_x$, Bi_2Se_3 , Bi_2Te_3 and Sb_2Te_3 were also realized^{5,6}. Over the last decade, the electronic properties of Bi_2Se_3 and Bi_2Te_3 have been extensively studied, with optimization of the properties of their topologically protected surface states. This has been carried out mainly by investigating the band structure of the surface electrons by imaging the band structure using angle resolved photoemission spectroscopy (ARPES)^{7,8}, including the spin-resolved variant, and time-resolved two-photon photoelectron (2PPE) spectroscopy⁹. Scanning tunneling microscopy (STM) can also be used to prove the existence of a linear dispersion relation and suppressed backscattering¹⁰.

To make use of these surface states in spintronics it is essential not only to demonstrate the existence of spin-polarized surface states but also to control them. One approach for controlling these surface states is to create an asymmetrically populated Dirac cone, which leads to spin-polarized currents on the surface due to spin-momentum locking. This idea has been realized for exfoliated Bi_2Se_3 ¹¹ and other materials and is enabled by the strong spin-orbit coupling in topological insulators such as Bi_2Se_3 lifting the spin degeneracy of the electrons in the surface states. As a result, the selection rules for interband transitions depend on the electron spin. Therefore, it is possible to use circular polarized light to selectively excite surface electrons with a parallel or antiparallel spin component with respect to the photon momentum and depending on the helicity. This creates an asymmetric population of the surface states in k -space, which due to the spin-momentum locking, leads to a spin-polarized electrical current (see FIG. 1 (a)). This effect of generating a spin-polarized charge current by creating an asymmetric carrier population in k -space by exciting optical transitions with circular polarized light imposed by optical selection rules is referred to as the circular photogalvanic effect and has been previously realized in semiconductor quantum wells¹².

More recently several studies have performed photocurrent measurements of the $\text{Bi}_{1-x}\text{Sb}_x$, Bi_2Se_3 , Bi_2Te_3 and Sb_2Te_3 group using photon wavelengths ranging from the visible to the terahertz or even up to the infrared regime^{13–15}. In this work, we demonstrate for the first time spin-polarized photogalvanic effects in Bi_2Se_3 nanowires with a cross-section in the nanometer range instead of in the micrometer-wide Hall bar structures used in previous experiments^{11,16}. The ratio of surface to bulk states in nanowires is higher and leads to an increased ra-

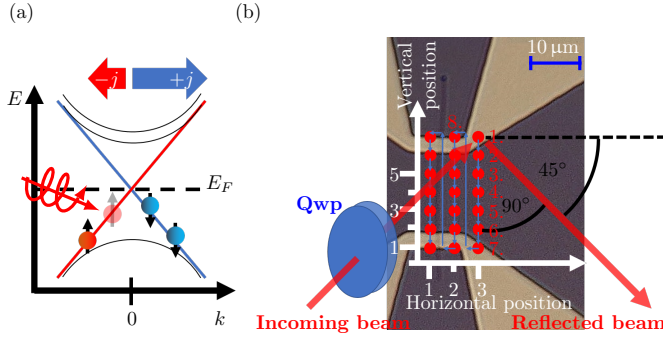


FIG. 1. (a) depicts a schematic band structure of Bi_2Se_3 in the presence of the circular photogalvanic effect. The asymmetric population of the surface states (implied by the unequal number of red and blue dots) is generated by the absorbed circular polarized light (red arrow) and generates a net spin-polarized electrical current due to the spin momentum locking. In (b), the raster pattern of the exciting laser beam as used in the experiment is displayed on the sample surface. The order of the laser spot positions is marked by red numbers. The angle of incidence of the laser light is fixed at 45° .

tio of spin-polarized currents to photocurrents originating from the bulk states.

The Bi_2Se_3 nanowires were synthesized by Au-catalyzed vapor-liquid-solid method on a Si(111) substrate (as described here:¹⁷). The cross-section of the nanowires is either rectangular or trapezoidal, resulting from the layered crystal structure. The width of the nanowires is on the scale of 50 nm and the thickness is in the range of 50 nm – 150 nm. The length can be as long as several tens of micrometers. The nanowire presented in FIG. 2 (a) has a total length of 36 μm . The Bi_2Se_3 nanowires are grown in the [110] direction as a single-crystal structure and have a smooth surface. The chemical composition can be characterized by an energy dispersive spectrometer in the scanning TEM mode. The measured ratio is 2:3 as expected for Bi_2Se_3 . The grown nanowires are mechanically transferred onto a Si (111) substrate, and the gold contacts separated by a 14 μm gap are fabricated on top of the nanowire by lithography. FIG. 2 (a) shows a micrograph of one of the nanowire devices with two contacts, which are each connected to two gold pads on the left- and on the right-hand sides of the nanowire¹⁸. The sample is mounted with silver paste onto a chip carrier and connected with 25 nm diameter gold wires by wire bonding.

The light source for the photocurrent measurements is a diode laser with a wavelength of 785 nm (1.55 eV) modulated at a frequency of 77 Hz. The laser light passes through a linear polarizer and a quarter-wave plate (qwp) prior to impinging on the sample surface under an angle of incidence of 45° . The rotation angle α of the qwp is controlled by a step motor to change the polarization of the excitation beam. The laser light is focused down to $(4.3 \pm 0.11) \mu\text{m} \times (2.89 \pm 0.08) \mu\text{m}$ on the sample sur-

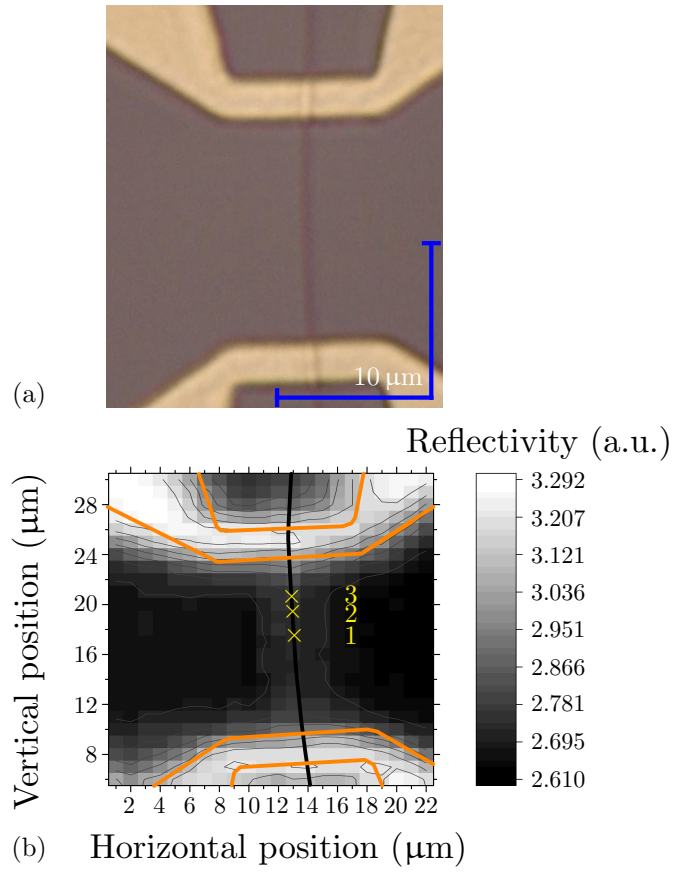


FIG. 2. (a) Shows a light microscopy image of the sample. A nanowire (dark gray vertical line) is placed on a Si (111) substrate (gray) and underneath gold contacts (yellow). The two closer parallel edges of the gold contacts are separated by 14 μm . (b) The edges of the gold contacts (orange) and the position of the nanowire (black line) are marked on the spatially resolved reflected light intensity. Three positions on the nanowire are marked and numbered by 1, 2 and 3.

face. The intensity of the light reflected from the sample surface is measured by a photodiode. The photocurrent between the two contacts and the light reflected from the sample surface are simultaneously measured by a lock-in amplifier. The laser spot can be moved across the sample surface along the vertical and horizontal directions by two step motors with a minimum step size smaller than 1 μm with an error of 200 nm. The raster pattern of the laser spot (red dots) is depicted in FIG. 1(b), as drawn on a light microscopy image of the sample. The measurement starts with the laser spot in the right upper corner (position 1 in FIG. 1(b)). Then the qwp is rotated by $\Delta\alpha = 6^\circ$ steps to carry out a full rotation while the photovoltage and the intensity of the reflected beam are measured. Afterwards, the laser spot is moved to the next position according to the raster pattern in FIG. 1(b), repeating the measurement procedure until the bottom left position is reached.

For each data point in the two-dimensional voltage

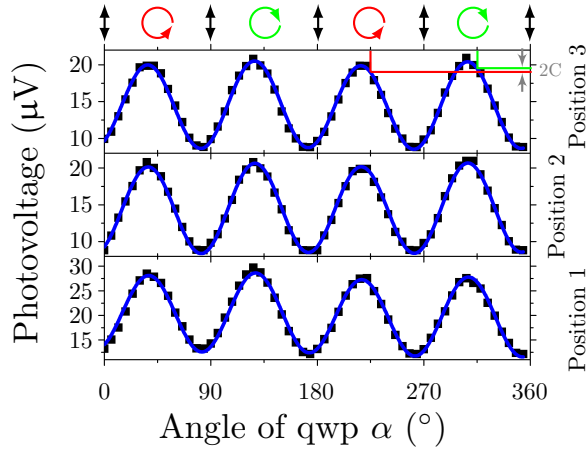


FIG. 3. The measured voltage (black squares) and the analysis results using eq. (1) (blue line) as a function of the rotation angle α for three laser spot positions (see FIG. 2 (b)) are displayed. In addition, the photovoltages for left and right circular polarized light (indicated by green and red lines) are marked. The difference between these photovoltage values is equal to $2C$.

maps, the photovoltage between the two contacts is measured while the qwp is rotated by 360° in total, changing the polarization from linear polarized ($\alpha = 0^\circ$), to left-circular polarized ($\alpha = 45^\circ$), to linear polarized ($\alpha = 90^\circ$), to right-circular polarized ($\alpha = 135^\circ$), to linear polarized ($\alpha = 180^\circ$), to left-circular polarized ($\alpha = 225^\circ$) and so on and so forth. The measured photovoltage v is a sum of four different contributions

$$v(\alpha) = C \sin(2\alpha) + L_1 \sin(4\alpha) + L_2 \cos(4\alpha) + D. \quad (1)$$

The contributions can be distinguished by their dependence on the polarization of the exciting laser light. Eq. (1) has previously been introduced to separate the different contributions to photocurrent measurements in exfoliated Bi_2Se_3 Hall bar devices¹¹. The first term $C \sin(2\alpha)$ of Eq. (1) describes the amount of spin-polarized voltage generated by the circular photogalvanic effect since it modulates the difference in the photovoltage for left and right circular polarized light and is zero if the exciting light is linear polarized. In the following, the magnitude of the amplitude C , which is half of the difference between the photovoltage for different helicities (see Fig. 3), is used as a measure for the size of the spin-polarized voltage. The second term $L_1 \sin(4\alpha)$ and third term $L_2 \cos(4\alpha)$ describe the contributions that arise from the linear photogalvanic effect and the photon drag effect. The last term D is independent of the polarization and arises from the Seebeck effect. Since the laser spot is smaller than the distance between the gold contacts, it creates an overall temperature gradient that can change in direction and size as the laser spot is moved across the sample surface. The measured photovoltage is analyzed by Eq. (1) to separate the four contributions at every laser spot position. The horizontal and vertical

positions of the laser spot are then used as the spatial coordinates for the extracted amplitudes as in FIG. 4 for the thermoelectric contribution represented by D and the spin-polarized contribution represented by C . At the same time, the intensity of the reflected light for every value of the photovoltage is measured with a second lock-in amplifier. Instead of fitting Eq. (1) to the obtained values, we take the value for a fixed polarization at $\alpha = 0^\circ$ and again use the position of the laser spot as the coordinates for the reflectivity to obtain a two-dimensional map of the reflectivity (see FIG. 2 (b)) which allows us to identify the positions of the nanowires and the gold contacts.

In the reflectivity map (FIG. 2 (b)) three different areas can be distinguished. The area with the highest intensity (white) shows the position of the Au contacts, while the region with the lowest reflectivity (black) represents the 300 nm SiO_2 on top of the Si substrate. The nanowire can be clearly distinguished between the contacts (in dark gray). Its size looks exaggerated since its diameter (150 nm) is smaller than the spot size of the laser beam, so it acts as a scattering center. Therefore, the reflectivity map proves that the area shown in FIG. 2 (a) is illuminated and indicates the position of the nanowire. The nanowire is marked in the photovoltage maps (FIG. 4) by a black line.

The three selected photovoltage measurements in FIG. 3 at three different positions along the nanowire (marked in blue in FIG. 2 (b)) show good agreement between Eq. (1) and the measured voltage. It is also observed, that the thermoelectric contribution D , which is equal to the shift along the vertical direction, is at least one order of magnitude larger than the spin-polarized contribution C . The spatially resolved maps in FIG. 4 enable a more detailed inspection of the two contributions. The thermoelectric amplitude D (FIG. 4(a)) changes its sign from positive at the top electrode to negative at the lower electrode. Note that the thermoelectric current that creates the thermoelectric voltage is generated by two temperature gradients with opposite signs that point from the laser spot position towards the two colder contacts. Therefore, the position of the laser spot with respect to the contacts determines the size and sign of the thermoelectric voltage. When the laser spot is in the center between the contacts, the two temperature gradients cancel, and thus, the net temperature gradient and D vanish. In our measurements (FIG. 4(a)), the direction of the net temperature gradient is encoded in red and blue, corresponding to the gradients pointing towards the lower or upper contacts, respectively. At the vertical position of $13 \mu\text{m}$ in FIG. 4(a), the thermoelectric contribution D becomes zero. Once the laser spot is moved toward one of the electrodes, the net temperature gradient is non-zero, and a net current is generated by the Seebeck effect. The sign of the thermoelectric current changes from top to bottom since the direction of the net temperature gradient is reversed. Thus, the voltage of the contour plot in the vertical direction along the nanowire changes its sign

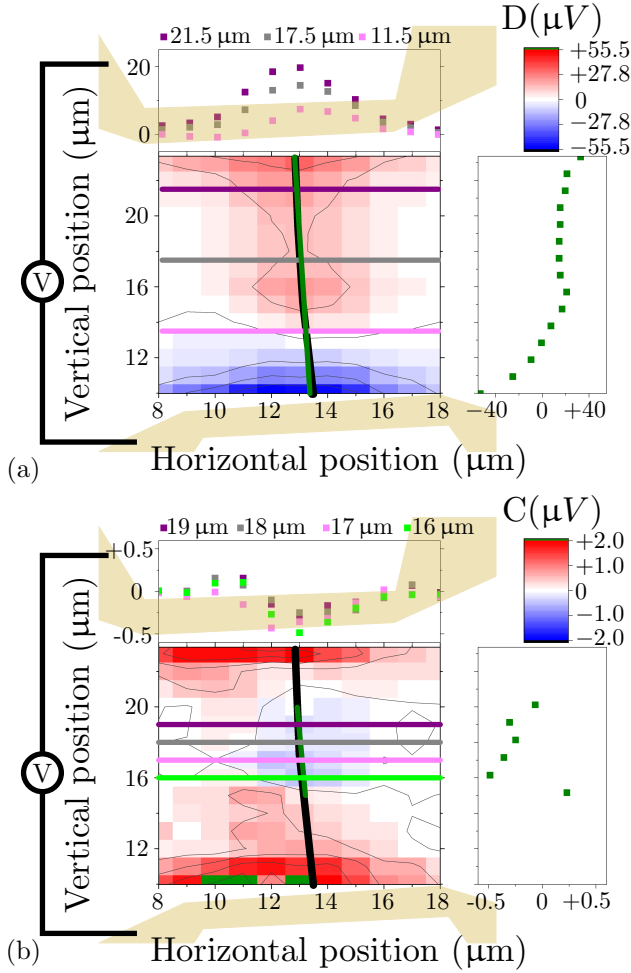


FIG. 4. (a) The map shows the amplitude D related to the thermoelectric voltage at different laser spot positions in the 14 μm gap between the gold contacts. The vertical contour plot shows the amplitude D along the nanowire position and the horizontal contour plots show how the thermoelectric voltage drops when the center of the laser spot is moved away from the nanowire. (b) The map shows the spatially resolved amplitude C , related to the spin-polarized current. The vertical contour plot shows the spin-polarized voltage along the nanowire (green line) and the four horizontal contour plots prove that the spin-polarized voltage increases when the nanowire is illuminated.

from top to bottom (shown in FIG. 4 (a)). The contour plots perpendicular to the nanowire reveal that the highest values for D are reached when the center of the laser spot matches the horizontal position of the nanowire at 13 μm . If the laser spot center is moved away from the nanowire along the horizontal direction, then the values decrease. When the laser spot center is 4 μm , which is equal to the full width at half maximum (FWHM) of the laser spot diameter, or further from the nanowire, the thermovoltage drops down to nearly zero. This means that there is no contribution to the thermoelectric contribution D transferred through the substrate.

A slight enhancement of the voltage is observed when not only the nanowire but also the nanowire underneath the gold contact is partially illuminated. This appears for the vertical positions above 22 μm and below 11 μm and is manifested by the nonlinear increase of the photovoltage in the vertical contour plot and also by the circular shape of the lines in the 2D map in FIG. 4 (a). This effect is also observed for measurements of GaN, ZnO and Si nanowires. In these materials, the observed increase is a result of the Schottky effect^{19–21}. In our case, the gold contact is metallic and the TI can act as a semiconducting layer. The sign of the current caused by the band bending at the metal/semiconductor interface changes between the contacts since the band bending is symmetrical with regard to the center of the nanowire; this is in good agreement with the behavior of the thermoelectric voltage D observed in this work.

To exclude the influence of the contacts, we focus on the spin-polarized contribution C in this work in the area between 15 and 20 μm along the vertical axes displayed in FIG. 4(b) in green. The contour plots along the horizontal direction show that the spin-polarized voltage C decreases when the center of the laser spot does not match the position of the nanowire at the horizontal position of 13 μm . This proves that the substrate does not contribute to the spin-polarized voltage. The largest value with a modulus of 0.5 μV is reached when the laser spot center matches the nanowire, which is a factor of 80 smaller than the largest value for the thermoelectric contribution $D = 40 \mu\text{V}$. The largest values are reached on the small plateau shown in the vertical contour plot over a range of 4 μm . Closer to the contacts, the spin-polarized voltage decreases.

In summary, we performed photocurrent measurements on Bi_2Se_3 nanowires and analyzed the spatially resolved results for the spin-polarized and thermoelectric contributions. For the thermoelectric contribution, we observe a sign change of D along and on the nanowire. In addition, we detect an enhancement of the thermoelectric and the spin-polarized contribution when the nanowire underneath the gold contacts is illuminated in comparison to illuminating only the TI. We also show that spin-polarized currents can be generated in nanowires within the range of 5 μm along the nanowire by using circular polarized light.

Thus, we have demonstrated the ability to drive photogalvanic currents in nanowires, which shows their promising potential for use in photo-spintronics applications in the future.

We are grateful to the German Science Foundation (DFG) for financial support through the priority program SPP1666: ‘Topological insulators: materials, fundamental properties, devices’ (MU1780/10-2).

¹C. L. Kane and E. J. Mele, “ Z_2 Topological Order and the Quantum Spin Hall Effect,” *Phys. Rev. Lett.* **95**, 146802 (2005).

²M. König, S. Wiedmann, C. Brüne, A. Roth, H. Buhmann, L. W. Molenkamp, X.-L. Qi, and S.-C. Zhang, “Quantum Spin Hall

- Insulator State in HgTe Quantum Wells,” *Science* **318**, 766–770 (2007).
- ³M. Z. Hasan and C. L. Kane, “Colloquium: Topological insulators,” *Rev. Mod. Phys.* **82**, 3045–3067 (2010).
- ⁴Y. Huang, Y. Song, S. Wang, I. Buyanova, and W. Chen, “Spin injection and helicity control of surface spin photocurrent in a three dimensional topological insulator,” *Nature Communications* **8**, 2041–1723 (2017).
- ⁵L. Plucinski, G. Mussler, J. Krumrain, A. Herdt, S. Suga, D. Grützmacher, and C. M. Schneider, “Robust surface electronic properties of topological insulators: Bi_2Te_3 films grown by molecular beam epitaxy,” *Applied Physics Letters* **98**, 222503 (2011).
- ⁶D. Biswas, S. Thakur, G. Balakrishnan, and K. Maiti, “Exceptional surface and bulk electronic structures in a topological insulator, Bi_2Se_3 ,” *Scientific Reports* **5** (2015).
- ⁷J. Krumrain, G. Mussler, S. Borisova, T. Stoica, L. Plucinski, C. Schneider, and D. Grützmacher, “MBE growth optimization of topological insulator Bi_2Te_3 films,” *Journal of Crystal Growth* **324**, 115–118 (2011).
- ⁸Z.-H. Pan, E. Vescovo, A. V. Fedorov, D. Gardner, Y. S. Lee, S. Chu, G. D. Gu, and T. Valla, “Electronic Structure of the Topological Insulator Bi_2Se_3 Using Angle-Resolved Photoemission Spectroscopy: Evidence for a Nearly Full Surface Spin Polarization,” *Phys. Rev. Lett.* **106**, 257004 (2011).
- ⁹J. Sobota, S.-L. Yang, D. Leuenberger, A. Kemper, J. Analytis, I. Fisher, P. Kirchmann, T. Devereaux, and Z.-X. Shen, “Ultrafast electron dynamics in the topological insulator Bi_2Se_3 studied by time-resolved photoemission spectroscopy,” *Journal of Electron Spectroscopy and Related Phenomena* **195**, 249 – 257 (2014).
- ¹⁰M. Romanowich, M.-S. Lee, D.-Y. Chung, S. D. Mahanti, M. G. Kanatzidis, and S. H. Tessmer, “Interplay of topological surface and bulk electronic states in Bi_2Se_3 ,” *Phys. Rev. B* **87**, 085310 (2013).
- ¹¹J. W. McIver, D. C. Hsieh, H. Steinberg, P. Jarillo-Herrero, and N. Gedik, “Control over topological insulator photocurrents with light polarization,” *Nature nanotechnology* **72**, 96–100 (2011).
- ¹²S. D. Ganichev and W. Prettl, “Spin photocurrents in quantum wells,” *Journal of Physics: Condensed Matter* **15**, R935–R983 (2003).
- ¹³K. N. Okada, N. Ogawa, R. Yoshimi, A. Tsukazaki, K. S. Takahashi, M. Kawasaki, and Y. Tokura, “Enhanced photogalvanic current in topological insulators via fermi energy tuning,” *Phys. Rev. B* **93**, 081403 (2016).
- ¹⁴H. Plank, S. N. Danilov, V. V. Bel’kov, V. A. Shalygin, J. Kampmeier, M. Lanius, G. Mussler, D. Grützmacher, and S. D. Ganichev, “Opto-electronic characterization of three dimensional topological insulators,” *Journal of Applied Physics* **120**, 165301 (2016).
- ¹⁵L. Braun, G. Mussler, A. Hruban, M. Konczykowski, T. Schumann, M. Wolf, M. Münzenberg, L. Perfetti, and T. Kampfrath, .
- ¹⁶T. Schumann, N. Meyer, G. Mussler, J. Kampmeier, D. Grützmacher, E. Schmoranzero, L. Braun, T. Kampfrath, J. Walowski, and M. Münzenberg, “Observation of spin Nernst photocurrents in topological insulators,” , arXiv:1810.12799 (2018).
- ¹⁷H. S. Shin, B. Hamdou, H. Reith, H. Osterhage, J. Gooth, C. Damm, B. Rellinghaus, E. Pippel, and K. Nielsch, “The surface-to-volume ratio: a key parameter in the thermoelectric transport of topological insulator Bi_2Se_3 nanowires,” *Nanoscale* **8**, 13552–13557 (2016).
- ¹⁸B. Hamdou, J. Gooth, A. Dorn, E. Pippel, and K. Nielsch, “Surface state dominated transport in topological insulator Bi_2Te_3 nanowires,” *Applied Physics Letters* **103**, 193107 (2013).
- ¹⁹F. Lonard, E. Song, Q. Li, B. Swartzentruber, J. A. Martinez, and G. T. Wang, “Simultaneous Thermoelectric and Optoelectronic Characterization of Individual Nanowires,” *Nano Letters* **15**, 8129–8135 (2015), PMID: 26529491.
- ²⁰C. Park, J. Lee, H.-M. So, and W. S. Chang, “An ultrafast response grating structural ZnO photodetector with back-to-back Schottky barriers produced by hydrothermal growth,” *J. Mater. Chem. C* **3**, 2737–2743 (2015).
- ²¹Y. Ahn, J. Dunning, and J. Park, “Scanning Photocurrent Imaging and Electronic Band Studies in Silicon Nanowire Field Effect Transistors,” *Nano Letters* **5**, 1367–1370 (2005).